THE DEPTH OF SIMPLE CRATERS AND THE PERMANENT SHADOW THEY CAST: EVIDENCE FOR ICE ON MERCURY BUT NOT ON THE MOON L. Rubanenko[1], J. Venkatraman[1], and D. A. Paige[1], [1]Department of Earth, Planetary and Space Sciences, UCLA, LA, CA 90095 (liorr@ucla.edu)

Introduction: The low obliquity of Mercury and the Moon causes the topography near their poles to cast persistent shadows. In the past, it was shown these permanently shadowed regions (PSRs) may trap volatiles, such as water ice, for geologic time periods [1, 13, 18]. On Mercury, evidence for the presence of water ice was remotely sensed in RADAR [7], reflectance [10] and visible imagery [4]. More recently, evidence for the presence of ice inside small craters ($\sim$ 1 km) and micro cold-traps ($1 - 10$ m) was found using data obtained by the Mercury Laser Altimeter (MLA) [5, 15]. In contrast, lunar cold-traps were not observed to contain significant ice quantities. While evidence for a thin, possibly micrometer-thick layer of ice was found in several lunar craters such as Shackelton [19], Earth-based RADAR observations did not detect areas > 1 km^2 with high backscattering [17], indicating that any existing ice must be thinner than a few decimeters or is in the form of distributed grains [3]. Here we constrain the ice thickness delivery rate using a statistical approach; we measure the depths of small craters (diameters $3 - 15$ km) on both bodies, and compare it to the depths these craters would have had if they were filled with ice. If the cold-trap volatile outflux is greater than the volatile influx, the craters depth should remain constant with latitude, as no ice accumulates inside them. If the influx is greater than the outflux, with time ice should accumulate inside craters, making them shallower.

Methods: First, we measure the crater depth to diameter (d/D) ratios on Mercury and the Moon. We begin by visually identifying small ($3 - 15$ km), simple craters on the Mercury Dual Imaging System (MDIS) and the Lunar Reconnaissance Orbiter Camera (LROC) global basemaps. Then, we manually measure the crater elevation along a south-north profile on the gridded MLA polar map (resolution of 250 m/px) and gridded Lunar Orbiter Laser Altimeter (LOLA, resolution of 100 m/px), as shown in Figure 1. On Mercury we measured craters between latitudes $75° - 86°$, where the most reliable MLA data is found. On the Moon, we measured craters in latitudes $78° - 87°$, and plan to extend this range to include both lower and higher latitudes. Overall, we measured 1003 craters on Mercury and 990 craters on the Moon. Next, we model the distribution these crater would have had if they were *filled* with ice up to the altitude of the PSR, and compare them with the measured distribution.

Crater Detection: After measuring the crater south-north topographic profile, we measured the crater dimensions using an algorithm we developed. First, we smooth the crater using a Gaussian filter. Then, we locate the crater rims by finding the maximum points in the left and right halves of the profile. The crater diameter is defined as the distance between the rims, its center is defined as the midpoint between the two rims, and its depth as the distance between the rims mean height and the height of the crater center. To verify the algorithm, we manually reviewed each crater in the database and corrected for computational errors.

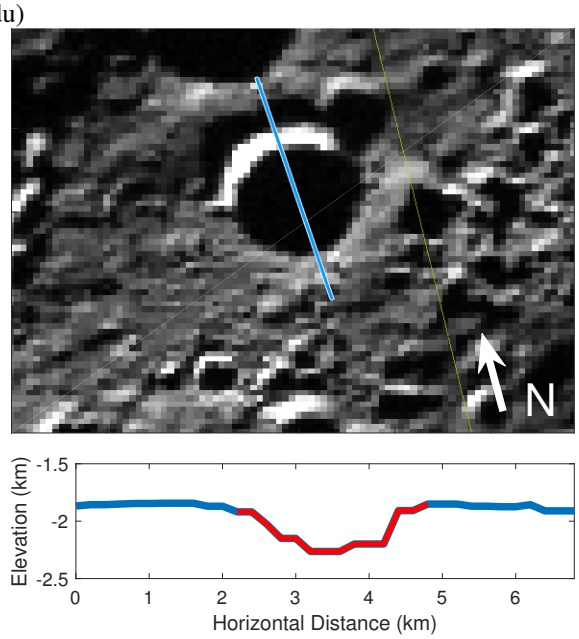

Figure 1: An example showing our method of measurement for one of the craters on Mercury. The blue line drawn on top of the crater in the top panel marks the the elevation profile shown in blue in the lower panel. The red line shows the crater that was identified using our detection algorithm.

Modeling the PSR Depth: Simple craters with diameters < 15 km can be approximated by hemispherical cavities [2, 8, 14]. As the Sun moves during the solar day the it illuminates different parts of the crater, causing it to cast transient shadows in different directions. Using trivial geometry, we calculate the depth of this transient shadow d_s cast at incidence angle θ_i,

$$\frac{d_s}{d} = \beta + \sin\theta_i \left(1 - \beta - \frac{\cot\theta_i}{2\Delta}\right) \quad (1)$$

where d is the crater depth and $\beta = (1 + 4\Delta^2)/8\Delta^2$, and where Δ is the crater d/D ratio (Figure 3). The depth of the permanent shadow is limited by the noontime transient shadow, which is the shallowest shadow cast during the solar day. For example, at latitude $80°$, a crater with d/D $\Delta = 0.1$ would cast a permanent shadow occupying 40% of its maximal depth. The depth of the PSR constrains the depth of ice accumulated inside the crater. Therefore, if we subtract the modeled PSR depth from the measured d/D in lower latitudes (where only a small amount of ice is expected to persist [12, 13, 16]) we should receive the d/D distribution of craters as if they were *filled with ice* up to the PSR limit. This assumes the

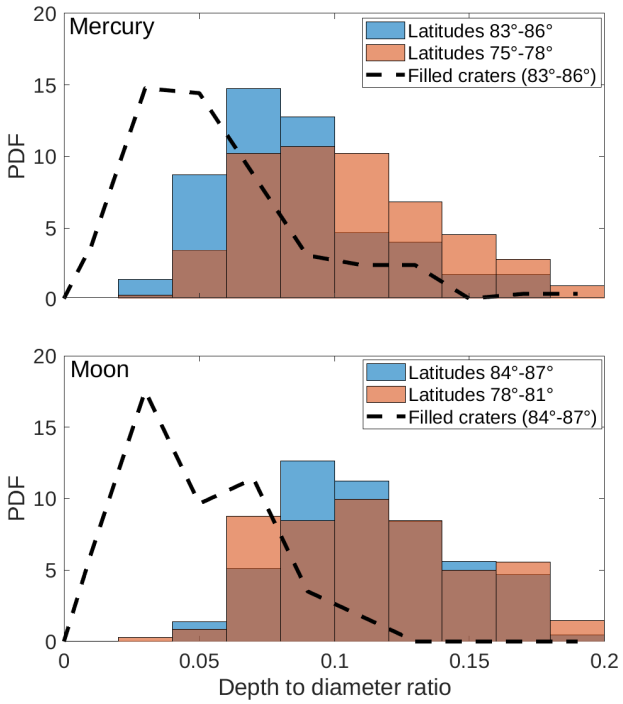

Figure 2: The d/D distributions of crater on Mercury (top) and the Moon (bottom), sampled at bins of width $\Delta = 0.02$. The bars show the measured values and the black line shows the modeled PSR depth value.

d/D in both does not significantly change with latitude due to some other inherent geologic property.

Results: Figure 2 shows the d/D distribution for Mercury (bars, top panel) and the Moon (bars, bottom panel). The d/D ratio of craters on Mercury decreases with increasing latitude as shallower (< 0.1) craters replace deeper craters (> 0.1). The mean d/D decreases from 0.106 ± 0.036 in latitudes $75° - 78°$ to 0.086 ± 0.034 in latitudes $83° - 86°$. On the Moon, however, craters' depth remains relatively constant with latitude; the mean d/D decreases from 0.117 ± 0.038 in latitudes $78° - 81°$ to 0.114 ± 0.033 in latitudes $84° - 87°$. The values above are provided along with the standard deviation. Next, we compare the distribution of the measured craters d/D in high latitude to the modeled distribution of the filled craters. As explained above, the modeled distribution is created using the latitude probability density function (PDF) of the high latitude craters considering the PDF of the d/D of low latitude craters, where only a small amount of ice can accumulate. The modeled filled craters d/D distribution is shown as the black dashed line in Figure 2. We find that on Mercury, cold-traps in small craters in high latitudes are filled to roughly half of their ice capacity. This can be seen both by comparing the shape of the distribution in Figure 2 (top) and by calculating the mean d/D of the modeled distribution:

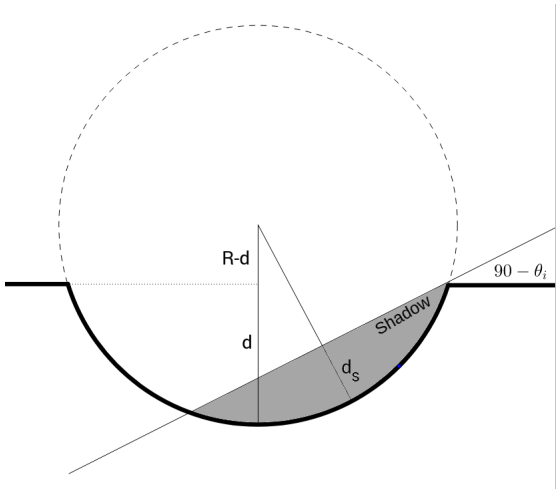

Figure 3: A sketch showing our PSR depth calculation. R is the radius of the circle defining the crater (bold line), d is the crater depth and d_s is the depth of the transient shadow at incidence angle θ_i.

0.059 ± 0.029; $\sim 30\%$ lower than the measured value shown above.

Discussion: Above we have shown the depth of small craters decreases with latitude on Mercury but not on the Moon. If this decrease is due to ice accumulation inside craters, this is another piece of evidence for the outstanding difference in ice quantities between the two bodies. On Mercury, craters become $\sim$ 20% shallower from latitudes $75° - 78°$ to $83° - 86°$. The mean crater depth in latitudes $75° - 78°$ is $\sim$ 400 m, which implies the infill is of order $\sim$ 10 − 100 m and a net delivery rate of $\sim$ 10 m Ga^{-1}, in accord with previous theoretical [9, 11] and observational [6] estimates. Additionally, the difference between the mean measured and modeled filled crater distributions indicates the historic mean volatile accumulation rate is greater - but probably of the same order - as the erosion rate.

References: [1] JR Arnold. *JGR* 84 (1979), 5659–5668. [2] D Buhl et al. *JGR* 73 (1968), 5281–5295. [3] BA Campbell et al. *Nature* 426.6963 (2003), 137–138. [4] NL Chabot et al. *Geology* 42 (2014), 1051–1054. [5] Ariel N Deutsch et al. *GRL* (2017). [6] Ariel N Deutsch et al. (2017). [7] JK Harmon et al. *Icarus* 149 (2001), 1–15. [8] AP Ingersoll et al. *Icarus* 100 (1992), 40–47. [9] JI Moses et al. *Icarus* 137.2 (1999), 197–221. [10] GA Neumann et al. *Science* 339 (2013), 296–300. [11] L Ong et al. *Icarus* 207.2 (2010), 578–589. [12] DA Paige et al. *Science* 330 (2010), 479–482. [13] DA Paige et al. *Science* 258 (1992), 643–646. [14] RJ Pike. *LPSC*. Vol. 8. 1977, 3427–3436. [15] L Rubanenko et al. (in review). [16] L Rubanenko et al. *Icarus* (2017). [17] NJS Stacy et al. *Science* 276.5318 (1997), 1527–1530. [18] K Watson et al. *JGR* 66 (1961), 3033–3045. [19] MT Zuber et al. *Nature* 486.7403 (2012), 378–381.